20th Australasian Fluid Mechanics Conference
Perth, Australia
5-8 December 2016

Characterisation of Overturning Flow in a Precessing Cylinder

T. Albrecht[1], P. Meunier[2], R. Manasseh[3], J. M. Lopez[4] and H. M. Blackburn[1]

[1]Department of Mechanical and Aerospace Engineering
Monash University, Victoria 3800, Australia

[2]IRPHE, CNRS, and Aix-Marseille Université, 13013 Marseille, France

[3]Department of Mechanical and Product Design Engineering
Swinburne University of Technology, Victoria 3122, Australia

[4]School of Mathematical & Statistical Sciences
Arizona State University, Tempe, AZ 85287, USA

Abstract

Experiments of the flow in precessing containers have repeatedly shown a rapid breakdown to turbulence, which remains unexplained to date. We present direct numerical simulations closely modelled after the experiments of Manasseh (JFM **243**, 1992). Despite the four times lower Reynolds number of 4780, we still observe a transition with the same characteristics as in the experiment. Analysis of the flow state preceding the breakdown shows a relatively clean and simple overturning flow, and a strong azimuthal mean flow. Contrary to observations by Manasseh, we find no flow reversals before or during the breakdown.

Introduction

Rotating flows, important in many geophysical, astrophysical, and industrial applications, are known to undergo a rapid and energetic transition from a laminar to a turbulent state. Aptly named "catastrophic collapse", this transition has been demonstrated in many experiments over the last decades [11, 10, 5, 9], yet remains unexplained today. Competing theories on the underlying mechanism have been proposed [6, 7, 8]. The aim of our project is to find a conclusive answer. Figure 1(a-c) reproduces flow visualisations from Manasseh's experiments [10] which show the type-A collapse, the most predominant of seven regimes he identified, and which we focus on in the present paper.

The lowest Reynolds number studied by Manasseh was $Re = 19\,116$. Direct numerical simulation (DNS) at this Re is possible today, but computationally quite demanding. We present DNS at a lower $Re = 4780$, but otherwise matching parameters—which is not only cheaper to compute, it is also more likely to give a clearer picture of the dynamics. As we will see, transition at this Re still has all the characteristics of a catastrophic collapse, i.e., breakdown over just a few cylinder revolutions, occurring shortly after the initial tilt-over. Our main goal in the present paper is to understand the flow state preceding the collapse, as this is required to be able to explain the breakdown process.

A relatively simple way to force the collapse in a controlled manner is precession, the rotation around two axes. This is in fact the forcing mechanism used by Manasseh (1992), and the one we have employed in our DNS. Figure 2 shows a schematic: A fluid-filled cylinder of aspect ratio $\Gamma = H/R$ is rotating around its axis at an angular frequency $\mathbf{\Omega}_1$. A gimbal (not shown), mounted on a turntable, allows the cylinder to be tilted through a nutation angle α. The turntable is rotating at $\mathbf{\Omega}_2$.

Initially, the nutation angle α is zero and the fluid is in solid-body rotation. Following the tilt-over, two main flow com-

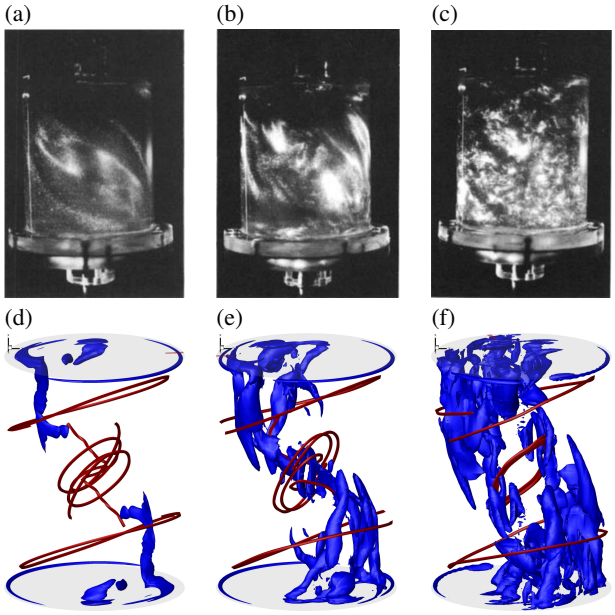

Figure 1: Top row: flow visualisation of the breakdown by pearlescent flakes, reproduced from Manasseh's precessing cylinder experiment. Frames (b) and (c) were taken 1.5 and 2.5 cylinder revolutions after frame (a), respectively. Bottom row: vortices identified by isosurfaces of λ_2, extracted from our DNS at corresponding intervals, i.e. (d) at $t/T_1 = 20.1$, (e) at $t/T_1 = 21.6$, (f) at $t/T_1 = 23.6$.

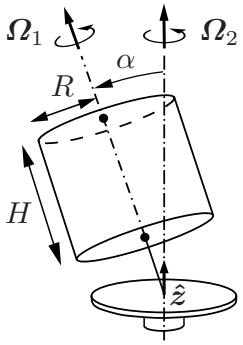

Figure 2: Schematic of the precessing flow.

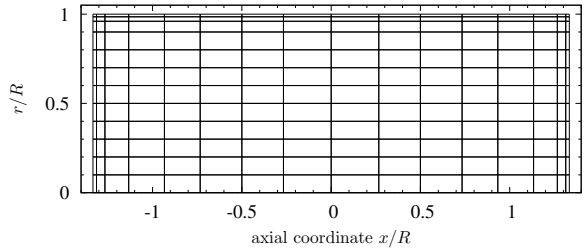

Figure 3: Spectral element mesh of the meridional semi-plane for a cylinder of height:radius ratio $\Gamma = 2.667$.

ponents develop. Firstly, precession directly forces an $m = 1$ flow, referred to as the forced mode. Shown in figure 6(a), it is an overturning flow initially rotating around the positive y-axis. Self-interaction of the forced mode, and interaction with other $m = 1$ components, then generates the second feature, an axisymmetric mean streaming flow, mainly in azimuthal direction. Via a yet-to-be-determined instability, the flow undergoes transition to turbulence within O(10) cylinder revolutions after the tilt-over.

Our paper will focus on the evolution of these two features before the collapse, in terms of mode shapes and temporal behaviour. Also, we are interested in an apparent reversal of the overturning flow, as reported by Manasseh at later stages of the breakdown.

Numerical Methods

The computational methodology utilises a spectral element–Fourier method for the incompressible Navier–Stokes equations [3]. The governing equations are solved in the gimbal frame of reference which, after the initial tilt-over, is rotating steadily at $\boldsymbol{\Omega}_2$ (cf. figure 2). The system was non-dimensionalised using the cylinder radius R as the length scale, and the cylinder rotation rate $1/\Omega_1$ as the time scale. Purely for convenience of describing the numerical method, we introduce cylindrical coordinates $\boldsymbol{r}$ in which radial, azimuthal, and axial velocity components (u,v,w) = $\boldsymbol{u}$, but stress that Cartesian coordinates will be used later as they are more adequate for most of the analysis presented in the results section. The non-dimensional governing equations are

$$\frac{\partial \boldsymbol{u}}{\partial t} + \boldsymbol{u}\cdot\boldsymbol{\nabla}\boldsymbol{u} + \frac{2}{\Omega_1}\boldsymbol{\Omega}_2\times\boldsymbol{u} + \frac{1}{\Omega_1}\frac{\mathrm{d}\boldsymbol{\Omega}_2}{\mathrm{d}t}\times\boldsymbol{r} = -\boldsymbol{\nabla}p + \frac{1}{Re}\nabla^2\boldsymbol{u}, \quad \text{with} \quad \boldsymbol{\nabla}\cdot\boldsymbol{u} = 0, \quad (1)$$

where any terms that can be written as gradients of a scalar are absorbed into the pressure gradient term, and p is the reduced pressure. Boundary conditions on all cylinder walls are $u = w = 0$ and $v = r$, and the initial condition is solid-body rotation, $(u,v,w) = (0,r,0)$, where r is the radial coordinate.

The spectral element mesh used had 192 spectral elements covering the meridional semi-plane, as shown in figure 3, and 128 data planes (64 Fourier modes) in azimuth. Local mesh refinement is concentrated near the walls to resolve the boundary-layer structure. Sixth-order tensor-product nodal basis functions are used in each element, giving at total of 7081 independent mesh nodes for each data plane and 906 368 nodes in total. We have checked this resolution is adequate to resolve flows for the parameters employed. Also, excellent agreement has been obtained previously between our DNS and time-averaged PIV data [2], and between DNS and theory [1].

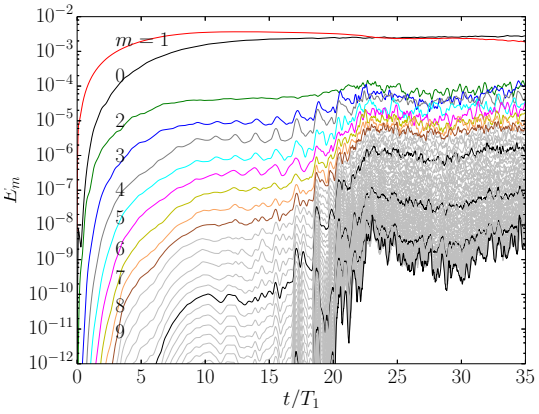

Figure 4: Kinetic energy in azimuthal Fourier modes

Results

As mentioned in above, Cartesian coordinates are more adequate for the analysis presented in the following. We will therefore use a Cartesian coordinate system attached to the gimbal, with x aligned with the cylinder axis and y pointing in the direction of $\boldsymbol{\Omega}_2 \times \boldsymbol{\Omega}_1$. All results presented here were obtained for a cylinder of aspect ratio $\Gamma = 2.667$, forced at a non-dimensional frequency $\omega = \Omega_1/(\Omega_1 + \Omega_2\cos\alpha) = 0.735$, which corresponds to the first resonance of the fundamental Kelvin mode (for details on Kelvin modes and their resonances, see, e.g. [12] or [1]). The tilt angle was $\alpha = 3°$, and the Reynolds number $Re = \Omega_1 R^2/\nu = 4780$. We have computed the flow in the gimbal frame of reference, in which $\boldsymbol{\Omega} = (\Omega_2^x, 0, \Omega_2^z)^T$ is steady after the initial tilt-over. Therefore, the forced mode is non-rotating, which simplifies analysis of the flow. For post-processing, we have removed the solid-body rotation (SBR) component, unless otherwise noted. Also note that due to the small nutation angle α, the component $\Omega_2^x = \Omega_2\cos\alpha$ is much larger than $\Omega_2^z = \Omega_2\sin\alpha$.

Fourier modal energy

To give an overview of the flow's general evolution, figure 4 shows history of kinetic energy in azimuthal Fourier modes. We can clearly see four phases: (i) the initial establishment of the forced mode over the first 10 revolutions, followed by (ii) a phase $10 \le t/T_1 \le 15$ during which modal energy is relatively flat on average, but overlaid by developing oscillations of a period of ≈ 1.7 cylinder revolutions. These oscillations seem to emerge first in modes $m \approx 4$; we have observed similar ones during the transition at larger nutation angle $\alpha = 15°$, but lower aspect ratio $\Gamma = 1.835$ [2]. Around $t/T_1 = 15$, growth of higher modes marks phase (iii), leading to the collapse at $t/T_1 \approx 23$ after which the flow remains turbulent (iv).

Flow structures and breakdown times

In order to confirm that our DNS captures a catastrophic collapse despite the lower Reynolds number, we compare experimental and numerical flow structures in figure 1. In the experiment, pearlescent flakes were illuminated in a meridional plane. For the simulation, we show vortices identified by the λ_2 criterion [4] (blue) and instantaneous streamlines (red). Frames (b,e) were taken 1.5 cylinder revolutions after (a,d); frames (c,f) another revolution after that.

Despite the different visualisation techniques, we observe very similar shapes and dynamics. With the onset of forcing, symmetric structures aligned along an S-shaped diagonal emerge. The core—shown by the inner streamlines—rapidly inclines to

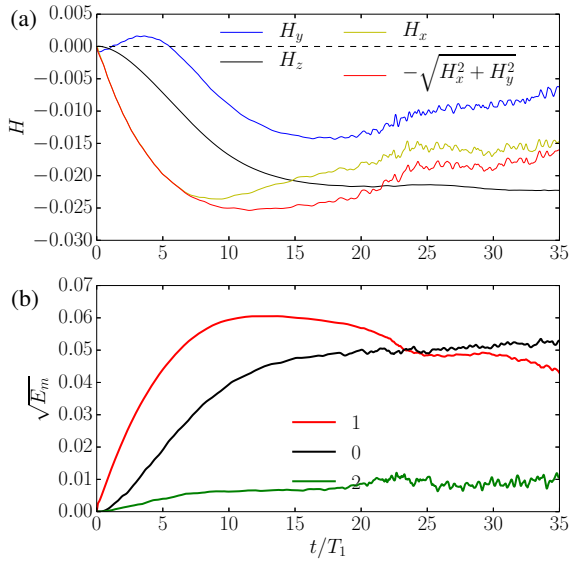

Figure 5: History of the Cartesian components of integral angular momentum. The axial component H_z tracks kinetic energy E_m in Fourier mode $m=0$, and the sum $(H_x^2+H_y^2)^{(1/2)}$ tracks energy in $m=1$. The ratio H_x/H_y is a proxy for the orientation angle of the overturning flow.

a 45° angle in both front and side view, as shown in figure 1(a) and (d). After just 1.5 cylinder revolutions, smaller scale structures appear in the core and in the corners (b,e). After another revolution, turbulence fills the whole container in the experiment (c); slightly less so in the DNS (f). In general, a larger scale of the structures in the DNS as compared to the experiment is expected due to the lower *Re*.

Breakdown times in the experiment (measured from commencement of forcing until the flow had reached its most disordered state) varied between 8 and 12 cylinder revolutions, depending on *Re*. In our DNS, the breakdown occurs considerably later, after 23 cylinder revolutions, on account of the lower Reynolds number and/or the lack of noise. The breakdown *duration* however, as demonstrated in figure 1, is fairly comparable. From these visual comparisons we may conclude that our DNS does capture a catastrophic collapse.

Overturning flow before the collapse

In order to be able to explain the collapse, we first need to understand the flow state preceding it. Therefore, we focus on phases (i) and (ii) in the following, i.e. times $t/T_1 < 23$, for which we characterise the evolution of the overturning flow, also in relation to the mean streaming flow. In particular, we are interested if there are any reversals as reported by Manasseh (1992).

To this end, we have extracted the volume integral of angular momentum after solid-body rotation has been removed,

$$\boldsymbol{H} = \int_v \boldsymbol{x} \times (\boldsymbol{u} - \boldsymbol{u}_{\mathrm{SBR}})\,\mathrm{d}v\,, \qquad (2)$$

the history of which is plotted in figure 5(a). Components of the vector quantity $\boldsymbol{H}$ can be interpreted as an amplitude of the flow rotating around the respective Cartesian axis. The black line in (a), H_z, represents net mean azimuthal flow; it is essentially a proxy for the square root of kinetic energy in azimuthal mode $m=0$ (plotted in figure 5b on a linear axis), because that energy is dominated by azimuthal flow. The other two components, H_x and H_y, represent overturning flow, and a sign change in both would signal a complete reversal of the total overturning flow. Also, the ratio H_x/H_y is a proxy for the orientation angle (around the cylinder axis) of the overturning flow. As expected, the sum $(H_x^2+H_y^2)^{(1/2)}$ closely tracks kinetic energy in Fourier mode 1 (cf. red lines in (a) and (b)).

The first component to emerge after the tilt-over is H_x (yellow line in a). This rotation around the positive y-axis is expected as a direct consequence of precessional forcing. The blue line in figure 5(a), H_y, is an overturning flow around z; it starts out slightly negative, then rises to a small positive maximum at $t/T_1 = 3.5$, followed by a decline until $t/T_1 = 17$. Streamlines in figure 6(a) visualise the early overturning flow at the time of the small maximum in H_y; dominance of H_x is evident. Some axial shear can be seen. This is caused by the azimuthal mean streaming flow, whose magnitude is about 30% of the overturning flow at this point in time (cf. H_z and H_y at $t/T_1 = 3.5$ in figure 5a). For comparison, we have removed the shear component in the bottom panels in figure 6. The strongest shear is observed near the end walls, but this is not an effect of boundary layers. In fact, we have chosen streamlines such that they do not penetrate boundary layers at all. Also, the streamline bending in figure 6(a-c) is consistent with contours of the mean streaming flow, shown in figure 7 for corresponding times.

By the time the overturning flow is deflected the most ($t/T_1 = 17$, when H_y has a negative maximum), the mean streaming flow has grown almost as large as the overturning flow, and a very strong shear is visible in figure 6(b). This is when kinetic energy in higher Fourier modes rises steeply and the collapse begins. Subsequently, the amplitude of the total overturning flow decreases, but retains broadly the same orientation (cf. figure 5(a) for $t/T_1 > 20$). Other than the initial transient in H_y, the integral angular momentum indicates no flow reversal in any component before, during, or after the breakdown, up until $t/T_1 = 35$ when the simulation was stopped. We note, however, that results at this time are not statistically stable, and the trend towards zero in H_y (cf. figure 5a) may continue. A longer simulation, currently underway, will clarify.

Discussion

In an attempt to explain some of the observed components of overturning flow, we now analyse conceptually how the Coriolis force—the body force which drives the flow—changes over time. These changes are either due to a change in orientation and/or magnitude of Ω, as is the case during the tilt-over, or due to a change in the velocity field $\boldsymbol{u}$. The idea is that any additional flow component $\boldsymbol{u}_\Delta$ linearly creates an additional part of the Coriolis force $-2\Omega \times \boldsymbol{u}_\Delta$. Analysing the direction and order of magnitude of the additional force may help us to anticipate how the flow will respond, at least initially. For this discussion, it is useful to recall that $\boldsymbol{\Omega}_2 = \boldsymbol{\Omega}_2^x + \boldsymbol{\Omega}_2^z$ has two parts of different magnitude, i.e. $\boldsymbol{\Omega}_2^x \gg \boldsymbol{\Omega}_2^z$, as a consequence of the small nutation angle.

As already mentioned in the results section, the overturning around the y-axis (H_y, yellow line in figure 5a) is a direct result of precession. More precisely, it is due to the divergence-free part of the initial body force $-2\boldsymbol{\Omega}_2^z \times \boldsymbol{u}_{\mathrm{SBR}}$. Note that the other part $-2\boldsymbol{\Omega}_2^x \times \boldsymbol{u}_{\mathrm{SBR}}$ is irrotational and therefore balanced by pressure.

The initial, slightly negative value of H_z can be explained by the Euler force $-\partial_t \boldsymbol{\Omega}_2 \times \boldsymbol{r}$ being non-zero for the (very short) duration of the tilt. The subsequent, brief rise in H_y may be due to the growing forced mode $\boldsymbol{u}_1$. The forced mode creates an additional and growing part $-2\boldsymbol{\Omega}_2^x \times \boldsymbol{u}_1$ of the Coriolis force. Although this secondary flow is much smaller than the background solid-body rotation, $\boldsymbol{u}_1 \ll \boldsymbol{u}_{\mathrm{SBR}}$, the resulting additional

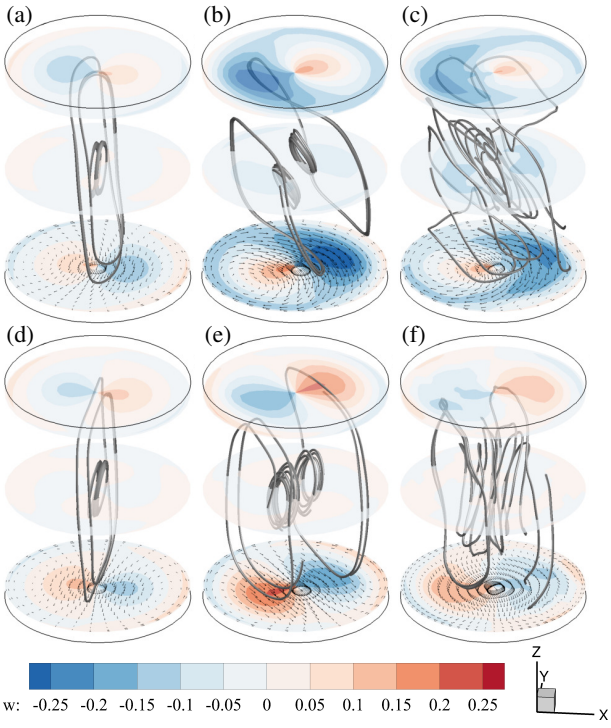

Figure 6: Evolution of streamlines and azimuthal velocity (contours in the centre plane and planes close to the end walls, but outside boundary layers) for $\alpha = 3^\circ$. (a) at $t/T_1 = 3.5$ where H_y has a positive maximum, (b) at $t/T_1 = 17$ where H_y has a negative maximum, and (c) at $t/T_1 = 35$, after the collapse. (d-f) as in (a-c), but with $m = 0$ component (shear) removed. Velocity vectors in the lower plane indicate the direction of rotation.

Coriolis force is of the same order as $-2\boldsymbol{\Omega}_2^z \times \boldsymbol{u}_{\mathrm{SBR}}$, because $\boldsymbol{\Omega}_2^x \gg \boldsymbol{\Omega}_2^z$ (for the same reason, the other part $-2\boldsymbol{\Omega}_2^z \times \boldsymbol{u}_1$ is negligible). However, we realise that the interaction of nonlinear, Coriolis, pressure gradient, and viscous terms, the balance of which ultimately determines the velocity field, is likely to be complex. Also, the above reasoning fails to explain the subsequent drop in H_y.

Conclusions

We have presented DNS of the type-A collapse, closely modelled after Manasseh's precessing cylinder experiment [10], although at a four times lower Reynolds number. We observe very similar flow structures and breakdown times, confirming Manasseh's observation that the collapse is rather insensitive to Reynolds number. In fact, our latest simulations, details of which we will report on in a future paper, still show a collapse at Reynolds numbers as low as $Re = 2570$. Also, the collapse is always preceded by the same characteristic pulses in the higher modes' energies as shown in figure 4, which suggests these pulses might play a crucial part in the breakdown mechanism.

Another interesting outcome of our study is that up until the collapse, the total flow basically only consists of a clean and relatively simple overturning flow whose orientation gradually changes, plus a strong azimuthal mean streaming flow. Generation of mean streaming in rotating flows is an interesting and important topic in itself, way beyond the scope of the present paper, and subject to ongoing research.

Existence of flow reversals, observed by Manasseh [10] at later stages of the breakdown, is not confirmed by our DNS. This could be simply because our simulations did not run long enough for a reversal to manifest. Also, the experimental flake visualisation in a single meridional plane might have been misleading.

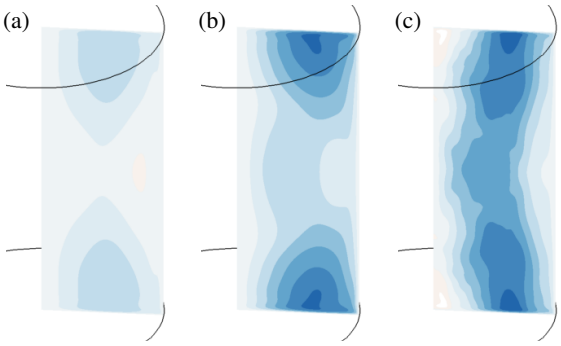

Figure 7: Instantaneous axisymmetric azimuthal velocity, for the same time instants shown in figure 6.

References

[1] Albrecht, T., Blackburn, H. M., Lopez, J. M., Manasseh, R. and Meunier, P., Triadic resonances in precessing rapidly rotating cylinder flows, *J. Fluid Mech.*, **778**, 2015, R1.

[2] Albrecht, T., Blackburn, H. M., Meunier, P., Manasseh, R. and Lopez, J. M., Experimental and numerical investigation of a strongly-forced precessing cylinder flow, *International Journal of Heat and Fluid Flow*.

[3] Blackburn, H. M. and Sherwin, S. J., Formulation of a Galerkin spectral element–Fourier method for three-dimensional incompressible flows in cylindrical geometries, *J. Comput. Phys.*, **197**, 2004, 759–778.

[4] Jeong, J. and Hussain, F., On the identification of a vortex, *J. Fluid Mech.*, **285**, 1995, 69–94.

[5] Johnson, L., The precessing cylinder, Notes on the 1967 Summer Study Program in Geophysical Fluid Dynamics at the Woods Hole Oceanographic Inst. Ref. 67–54, 1967.

[6] Kerswell, R. R., Secondary instabilities in rapidly rotating fluids: inertial wave breakdown, *J. Fluid Mech.*, **382**, 1999, 283–306.

[7] Kobine, J. J., Inertial wave dynamics in a rotating and precessing cylinder, *J. Fluid Mech.*, **303**, 1995, 233–252.

[8] Kobine, J. J., Azimuthal flow associated with inertial wave resonance in a precessing cylinder, *J. Fluid Mech.*, **319**, 1996, 387–406.

[9] Malkus, W. V. R., Precession of the Earth as the cause of geomegnetism, *Science*, **160**, 1968, 259–264.

[10] Manasseh, R., Breakdown regimes of inertia waves in a precessing cylinder, *J. Fluid Mech.*, **243**, 1992, 261–296.

[11] McEwan, A. D., Inertial oscillations in a rotating fluid cylinder, *J. Fluid Mech.*, **40**, 1970, 603–640.

[12] Meunier, P., Eloy, C., Lagrange, R. and Nadal, F., A rotating fluid cylinder subject to weak precession, *J. Fluid Mech.*, **599**, 2008, 405–440.